



HAL
open science

Irradiated UAmO₂ transmutation discs analyses: from dissolution to accurate isotopic analyses

Alexandre Quemet, Emilie Buravand, Jean-Gabriel Peres, Vincent Dalier,
Syriac Bejaoui

► **To cite this version:**

Alexandre Quemet, Emilie Buravand, Jean-Gabriel Peres, Vincent Dalier, Syriac Bejaoui. Irradiated UAmO₂ transmutation discs analyses: from dissolution to accurate isotopic analyses. *Journal of Radioanalytical and Nuclear Chemistry*, 2022, pp.10.1007/s10967-021-08156-2. 10.1007/s10967-021-08156-2 . cea-03516347

HAL Id: cea-03516347

<https://cea.hal.science/cea-03516347>

Submitted on 7 Jan 2022

HAL is a multi-disciplinary open access archive for the deposit and dissemination of scientific research documents, whether they are published or not. The documents may come from teaching and research institutions in France or abroad, or from public or private research centers.

L'archive ouverte pluridisciplinaire **HAL**, est destinée au dépôt et à la diffusion de documents scientifiques de niveau recherche, publiés ou non, émanant des établissements d'enseignement et de recherche français ou étrangers, des laboratoires publics ou privés.

1 Names of the authors: Alexandre Quemet¹, Emilie Buravand¹, Jean-Gabriel Peres¹,
2 Vincent Dalier¹ and Syriac Bejaoui²

3 Title: Irradiated UAmO₂ transmutation discs analyses: from dissolution to isotopic
4 analyses

5

6 Affiliation(s) and address(es) of the author(s):

7 - ¹ CEA, DES, ISEC, DMRC, Univ Montpellier, Marcoule, France

8 - ² CEA, DES, IRESNE, DEC, SESC, LECIM, F-13108 Saint-Paul-Lez-Durance,
9 France

10 E-mail address of the corresponding author: alexandre.quemet@cea.fr

11

12 **Irradiated UAmO₂ transmutation discs analyses: from**
13 **dissolution to isotopic analyses**

14 *Alexandre Quemet¹, Emilie Buravand¹, Jean-Gabriel Peres¹, Vincent Dalier¹ and Syriac*
15 *Bejaoui²*

16 *¹ CEA, DES, DMRC, Univ Montpellier, Marcoule, France*

17 *² CEA, DES, IRESNE, DEC, SESC, LECIM, F-13108 Saint-Paul-Lez-Durance, France*

18 **Abstract**

19 This paper details the different steps for the isotopic determination of UAmO₂ discs from
20 analytical irradiation. MARIOS and DIAMINO irradiations were performed in materials
21 testing reactors to study the behaviour of americium bearing blanket samples in regard of
22 heterogeneous recycling in sodium-cooled fast reactor. Six irradiated discs were dissolved
23 in hot cells and were analyzed to determine isotope ratios of uranium, plutonium,
24 americium and neodymium. The ratios were measured combining chemical separations
25 and TIMS analyses. Using the double isotope dilution methodology helps measuring
26 ²³⁸Pu/²³⁸U, ²⁴¹Am/²³⁸U and ¹⁴⁸Nd/²³⁸U ratios with uncertainty about a few per mil (k = 2).

27 **Keywords**

28 TIMS, isotope ratio, isotope dilution, transmutation, ion exchange resin, HPLC

29

30 **Introduction**

31 Since 2008, the French Alternative Energies and Atomic Energy Commission (CEA)
32 started a program dedicated to study the americium recycling [1–4]. The R&D program is
33 devoted to develop actinide bearing blankets for transmutation in sodium-cooled fast
34 reactor. Two different kinds of fuel, containing americium, were manufactured in the
35 ATALANTE facility: $U_{0.85}Am_{0.15}O_2$ discs with dense and tailored porosity [5]. Two
36 separate-effect irradiation experiments were performed to understand the $UAmO_2$ discs
37 behavior under irradiation and to determine the americium transmutation yield. The
38 experiments were also devoted to study the influence of the microstructure on the gas
39 release as a function of temperature [1]. Indeed, a large quantity of helium is produced
40 under irradiation, mainly coming from the transmutation chain of ^{241}Am isotope, and could
41 lead to significant swelling and a pellet-cladding interaction. The first irradiation
42 experiment, called MARIOS, was implemented in the High Flux Reactor (Petten,
43 Netherland) from March 2011 until May 2012, and investigated temperatures ranged
44 between 1000 and 1200°C. The second experiment (DIAMINO irradiation) was irradiated
45 in the OSIRIS reactor (Saclay, France) from February 2014 until December 2015 and
46 focused on temperatures ranging between 600 and 800°C.

47 To obtain the transmutation yield and compare experimental results with neutronic
48 simulation codes, isotopic analyses after quantitative dissolution of the irradiated discs
49 were performed. Among these determinations, U, Pu, Am, Cm and Nd isotope
50 compositions must be obtained accurately (*i.e.* measurement trueness and precision).
51 Moreover, simulation codes require data on $^{238}Pu/^{238}U$, $^{241}Am/^{238}U$ and $^{148}Nd/^{238}U$ ratios.
52 In the nuclear fuel, the burn-up is monitored using stable or long-lived isotopes (*e.g.*
53 $^{148}Nd/^{238}U$ ratio) that are invariantly produced under most conditions: a certain amount of
54 each isotope is produced per fission occurring in the fuel. Six irradiated discs were
55 dissolved and dissolution solutions were analyzed in the ATALANTE facility: 2 from
56 MARIOS irradiation experiments [3] and 4 from DIAMINO irradiation experiments [1].
57 This study is focused on the U, Pu, $^{238}Pu/^{238}U$, $^{241}Am/^{238}U$ and $^{148}Nd/^{238}U$ isotope ratio
58 determination.

59 Spent fuels are commonly dissolved in hot nitric acid in reprocessing plants [6, 7].
60 Nevertheless, a mixture of nitric acid and hydrofluoric acid was used to ensure plutonium
61 quantitative dissolution in this study [6–8].

62 Thermal Ionization Mass Spectrometry (TIMS) is an instrument of choice for actinides and
63 lanthanides isotopic analysis with high accuracy [9–15]. Several artefacts disrupt the TIMS
64 measurements: isotope fractionation, abundance sensitivity or isobaric interferences.

65 Isotope fractionation comes from an evaporation difference between the light and the heavy
66 isotopes, causing a bias on measured isotope ratios. Different methodologies can be used
67 to overcome the isotope fractionation: internal or external normalization or the total
68 evaporation method (TE method). The TE method is generally used in the nuclear field to
69 obtain reference values of all the measured isotope ratios [16]. It is based on the evaporation
70 and the ionization of the entire sample. Therefore, the ion beam of the element is totally
71 collected by a multi-collection system. This method is barely affected by the isotope
72 fractionation and was successfully applied to U, Pu, Am or Nd [14, 17–19].

73 Minor isotope ratios analyses (*e.g.* $^{234}\text{U}/^{238}\text{U}$ or $^{236}\text{U}/^{238}\text{U}$) is more complicated due to low
74 signal or abundance sensitivity contribution. The abundance sensitivity (or peak tailing
75 effect) is the contribution of the major isotope peak tail (*e.g.* ^{235}U or ^{238}U) to the minor
76 isotope detection (*e.g.* ^{234}U or ^{236}U). Using Faraday cups coupled to a 10^{12} or 10^{13} Ω current
77 amplifier, instead of 10^{11} Ω , helps improving the TIMS sensibility [9]. For very low signal,
78 using Secondary Electron Multiplier (SEM) improves dramatically the TIMS sensitivity.,
79 Using the SEM coupled to a Retarding Potential Quadrupole Lenses improves the
80 measurement trueness by improving the abundance sensitivity. But, low SEM stability
81 renders low uncertainty measurements difficult. The TE method limits the $^{234}\text{U}/^{238}\text{U}$ or
82 $^{236}\text{U}/^{238}\text{U}$ ratios uncertainties to about few percent [17]. The development of a method with
83 multi-dynamic sequences allowing mathematical correction of the abundance sensitivity,
84 calibrating the SEM while the method is running and correcting isotope fractionation using
85 internal normalization improve the measurement trueness, the repeatability as well as the
86 uncertainties [17].

87 Isobaric interferences (e.g. $^{148}\text{Nd}/^{148}\text{Sm}$, $^{150}\text{Nd}/^{150}\text{Sm}$, $^{238}\text{U}/^{238}\text{Pu}$, $^{241}\text{Am}/^{241}\text{Pu}$ or
88 $^{242\text{m}}\text{Am}/^{242}\text{Pu}$) are another bias observed for TIMS measurements. Chemical separation
89 using ion exchange resin or High-Performance Liquid Chromatography (HPLC) is an
90 efficient method to reduce them. The separation on resin takes advantage of ion exchange
91 resins' different affinity with each element, according to its chemical species, its oxidation
92 state and the environment acidity. By putting the resin in contact with wisely chosen
93 eluents, it is possible to separate the species. The ion exchange resin TEVA (for
94 TEtraValent Actinides) and UTEVA (for Uranium and TEtraValent Actinides) are well
95 known to purify U, Pu and trivalent elements like Am [19–22]. The Am/Cm and the
96 lanthanide separation can be achieved using HPLC [16, 19, 23, 24]. Using optimal
97 separation conditions helps purifying Nd and Am in the same experiment [19].

98 Combining TIMS measurement and isotope dilution methodology (ID-TIMS) is a powerful
99 method for mass fraction determination [14, 25, 26]. $^{238}\text{Pu}/^{238}\text{U}$, $^{241}\text{Am}/^{238}\text{U}$ and $^{148}\text{Nd}/^{238}\text{U}$
100 ratios can be calculated using U, Pu, Am and Nd mass fractions obtained by ID-TIMS,
101 ^{238}U , ^{238}Pu , ^{241}Am and ^{148}Nd isotope abundances and molar masses. The $^{238}\text{Pu}/^{238}\text{U}$ ratio
102 uncertainty can be, in first approximation, estimated by propagating U and Pu mass fraction
103 uncertainties. Considering the U and Pu mass fraction measurement uncertainties in
104 safeguards nuclear materials using ID-TIMS in hot cell condition (0.84 %, $k = 2$) [27], the
105 $^{238}\text{Pu}/^{238}\text{U}$ ratio uncertainty will be estimated to 1.2 % ($k = 2$) using the propagation of
106 uncertainty [28]. $^{238}\text{Pu}/^{238}\text{U}$, $^{241}\text{Am}/^{238}\text{U}$ and $^{148}\text{Nd}/^{238}\text{U}$ ratios uncertainties will be limited
107 to few percent using the ID-TIMS methodology, which is not enough for neutronic
108 calculation validation.

109 The double isotope dilution (DID) methodology is another method to determine the ratio
110 between two isotopes of two elements present in a sample, with one of them used as a
111 reference [29]. As for the isotope dilution, this method is based on the addition of a spike
112 to the sample. The spike solution contains the same analytes as the sample with a different
113 isotope composition. For instance, for the $^{238}\text{Pu}/^{238}\text{U}$ ratio determination a spike enriched
114 with ^{235}U and ^{242}Pu isotopes is required. This spike must be certified for the $^{242}\text{Pu}/^{235}\text{U}$
115 ratio. The $^{238}\text{Pu}/^{242}\text{Pu}$ and $^{238}\text{U}/^{235}\text{U}$ ratios determination of the (sample – spike) mixture
116 reflect the $^{238}\text{Pu}/^{238}\text{U}$ ratio of the sample. The DID helps obtaining accurate measurements

117 as it is only based on isotope ratios determination. Separation yields and weights
118 uncertainties are not to be taken into account in such case.

119 This paper aims at detailing the different steps for the isotopic analyses of the irradiated
120 discs from the MARIOS and DIAMINO experiments. Methods and protocol optimization
121 for the accurate isotopic measurements performed by TIMS measurements will be detailed.
122 The same protocol was used for the 2 discs provided from the MARIOS irradiation
123 experiment and for the 4 discs provided from the DIAMINO irradiation experiment. The
124 results presented here focus more specifically on two of the discs: one from the MARIOS
125 experiment (hereafter referred to as MARIOS disc) and one from the DIAMINO
126 experiment (hereafter referred to as DIAMINO disc).

127 **Experimental**

128 Reagents and reference materials

129 The detailed information about reagents and reference materials can be seen in the
130 supplementary information. The U spike solution, enriched in ^{235}U isotope (93 %), was the
131 IRMM 054 certified reference material (CRM). The Pu spike solution, enriched in ^{242}Pu
132 isotope (95 %), was the IRMM 049d CRM. The Am spike solution, enriched in ^{243}Am
133 isotope (88 %), was the STAM CRM. The Nd spike solution, enriched in ^{150}Nd isotope,
134 was prepared by dissolving a ^{150}Nd enriched (95%) non-radioactive neodymium oxide
135 powder. This solution, hereafter referred to as ^{150}Nd spike solution, is not certified for
136 isotope ratios or mass fraction. The 3135a CRM (natural Nd), was used to determine the
137 ^{150}Nd spike mass fraction by reverse isotope dilution. The 3135a CRM is only certified for
138 the mass fraction (and not for isotope ratios). The IRMM 187 CRM was used for the
139 analytical method validation of $^{234}\text{U}/^{238}\text{U}$ and $^{236}\text{U}/^{238}\text{U}$ isotope ratios.

140 The samples analyzed during the “2017 Nuclear Material Round Robin” (hereafter referred
141 to as 2017NMRoRo) and during the “2019 Nuclear Material Round Robin” (hereafter
142 referred to as 2019NMRoRo) inter-laboratory comparisons (ILC) organized by the
143 International Atomic Energy Agency (IAEA) were used to estimate the uncertainties.

144 These ILC aim at determining U and Pu isotope ratios in a dried mixed Pu-U nitrate
145 samples for the 2019NMRoRo and in a Pu nitrate sample for the 2017NMRoRo. The Pu
146 nitrate sample supplied during the 2017NMRoRo ILC is hereafter referred to as 2017PuNH
147 sample. The Pu-U nitrate sample supplied during the 2019NMRoRo ILC is hereafter
148 referred to as 2019UPuNH sample.

149 The isotope ratios determined in this study were updated on 2019/10/01 to correct the
150 radioactive decay [30].

151 Separation experimental set-up

152 Three different separations using TEVA and UTEVA resins and HPLC were used. Each
153 separation protocol is detailed in the supplementary information. The TEVA and UTEVA
154 resins were used to obtain purified fractions of U, Pu and trivalent elements. The HPLC
155 separation were used to obtain purified fractions of Am and Nd [19].

156 Thermal Ionization Mass Spectrometer

157 The measurements were performed with the Thermo Scientific Triton TIMS equipped with
158 a glove box. The instrument is equipped with 9 Faraday cups (all are movables except the
159 central denoted C) which can be coupled to $10^{11} \Omega$ current amplifiers (8 available and
160 hereafter referred to as FC 11), $10^{12} \Omega$ current amplifier (1 available and hereafter referred
161 to as FC 12) or $10^{13} \Omega$ current amplifier (1 available and hereafter referred to as FC 13). 4
162 Faraday cups are positioned in low masses (noted L1–L4) and 4 Faraday cups are
163 positioned in high masses (noted H1–H4). The TIMS is also equipped with one fixed SEM,
164 equipped with a Retarding Potential Quadrupole Lenses and located behind the central
165 Faraday cup.

166 A double Re-filament configuration was used to control independently the evaporation and
167 the ionization temperature. These filaments (Re metal, purity 99.99 % and 99.999 %) are
168 provided by ATES (France) and were outgassed for 20 min at 4.5 A in a high vacuum
169 chamber ($<5 \times 10^{-6}$ mbar) before use. The 99.999 % purity was only dedicated for the

170 $^{234}\text{U}/^{238}\text{U}$ and $^{236}\text{U}/^{238}\text{U}$ ratios measurements. 1 μL was deposited onto the filament and
171 was dried with a 0.4 A current. After deposition, the current increased progressively to 2 A
172 in 10 seconds.

173 Isotopic analysis method

174 *Total evaporation method*

175 $^{235}\text{U}/^{238}\text{U}$, Pu, Am and Nd isotope ratios were measured using the TE method previously
176 described [14, 17–19]. In a nutshell, the TE method is divided in 3 phases: adjustment,
177 acquisition and shutdown phases. First, the ionization filament is heated to 5.5 A in 20 min
178 for Nd analyses and in 10 min for U, Pu and Am analyses. Then, the evaporation filament
179 is heated to obtain the major isotope ions beam of 1 mV. A “peak center” (mass calibration
180 and ions beam centering in the detector) and the lenses optimization of the ion source are
181 performed on the major isotope ion beam. In the second phase (acquisition phase), the data
182 acquisition is started. The evaporation filament current starts to increase until the ion beam
183 intensity of all measured isotopes reaches the target intensity. The evaporation filament is
184 then controlled to keep the ions beam intensity constant, by increasing the evaporation
185 current when necessary. When the evaporation filament current reaches a maximum value
186 of 6.5 A and the ion beam decreases down to a 25 mV signal, the data acquisition is then
187 finished (shutdown phase).

188 For the DID measurements, the isotopes (^{235}U , ^{238}U , ^{238}Pu , ^{242}Pu , ^{241}Am , ^{243}Am , ^{148}Nd and
189 ^{150}Nd) were measured using FC 11. For the $^{235}\text{U}/^{238}\text{U}$ isotope ratio determination, ^{235}U
190 isotope was detected using FC 12 and ^{238}U isotope was collected using FC 11. Mass 239
191 (^{239}Pu) was also measured to look for a possible Pu contamination using FC 11. For Pu
192 isotope ratios determination, ^{238}Pu , ^{240}Pu and ^{242}Pu isotopes were measured using FC 11,
193 ^{239}Pu isotope was detected with the FC 12 and ^{241}Pu was collected with the FC 13. Mass
194 235 (^{235}U) was also measured to look for a possible U contamination using FC 11.

195 *Classical method using multi-dynamic sequence*

196 $^{234}\text{U}/^{238}\text{U}$ and $^{236}\text{U}/^{238}\text{U}$ ratios were measured with the classical method using multi-
197 dynamic sequence (hereafter referred to as CMD method). The isotope fractionation was
198 overcome with an internal normalization using the $^{235}\text{U}/^{238}\text{U}$ ratio previously measured
199 with the TE method. The exponential law was used. Compare to the method previously
200 described [17], some parameters (integration number, measurement time and idle time)
201 were updated to take into account the use of the FC 13. Idle time using FC 13 must be
202 increased compared to the method using FC 12, to ensure that the Faraday cups response
203 return to their background level: time response of the FC 13 is slower than that of the
204 FC 12.

205 The updated parameters of the CMD method are summarized in Table 1. The CMD method
206 always includes 4 measurement sequences performed one after the other. In the first
207 sequence, the ^{234}U isotope was collected on the FC 13, the ^{235}U isotope was measured on
208 the FC 12, the ^{236}U isotope was collected on the SEM and the ^{238}U was collected on FC 11.
209 The measurement was performed with 3 integrations of 8 s. Sequence 2, dedicated to the
210 real-time SEM/FC inter-calibration, was performed using the SEM to measure the ^{234}U
211 isotope and a FC 11 to detect the ^{235}U isotope. The measurement was performed with 3
212 integrations of 8 s. The sequence 3 and 4 used the same detector configuration as the
213 sequence 1 and were dedicated to tailing contribution measurement. Each measurement
214 corresponds to 6 blocks of 10 cycles. Each cycle corresponds to the acquisition of the 4
215 measurement sequences presented in the Table 1.

216 Equations to calculate the $^{234}\text{U}/^{238}\text{U}$ isotope ratio corrected from the peak tailing and the
217 isotope fractionation, as well as the $^{236}\text{U}/^{238}\text{U}$ isotope ratio corrected from the peak tailing,
218 the SEM/FC inter-calibration gain and the isotope fractionation were previously explained
219 in details [17]. For the method validation with the updated parameters, 5 analyses were
220 performed on the IRMM 187 CRM.

221 Double isotope dilution

222 *Principle*

223 The X/²³⁸U ratios determination (X = ²³⁸Pu, ²⁴¹Am or ¹⁴⁸Nd) required using a spike
224 enriched with ²³⁵U and Y isotopes (Y = ²⁴²Pu, ²⁴³Am or ¹⁵⁰Nd) [31]. The Y/²³⁵U ratio of
225 the spike must be known. Then, the spike is mixed with the sample. The X/²³⁸U ratio in the
226 sample is calculated with the measurements of the X/Y and ²³⁸U/²³⁵U mixture ratios
227 (Eq. (1)).

$$\left(\frac{X}{^{238}\text{U}}\right)_S = \left(\frac{Y}{^{235}\text{U}}\right)_T \cdot \frac{\left[\left(\frac{X}{Y}\right)_M - \left(\frac{X}{Y}\right)_T\right] \cdot \left[1 - \left(\frac{^{238}\text{U}}{^{235}\text{U}}\right)_M \cdot \left(\frac{^{238}\text{U}}{^{235}\text{U}}\right)_S\right]}{\left[\left(\frac{^{238}\text{U}}{^{235}\text{U}}\right)_M - \left(\frac{^{238}\text{U}}{^{235}\text{U}}\right)_T\right] \cdot \left[1 - \left(\frac{X}{Y}\right)_M \cdot \left(\frac{Y}{X}\right)_S\right]} \quad (1)$$

228 Where *T* refers to the spike (or tracer), *M* refers to the (sample – spike) mixture and *S* refers
229 to the sample.

230 ²⁴²Pu/²³⁵U spike preparation

231 The spike enriched in ²³⁵U and ²⁴²Pu isotopes (hereafter referred to as ²⁴²Pu/²³⁵U spike),
232 required to measure the ²³⁸Pu/²³⁸U sample ratio, was prepared gravimetrically from
233 IRMM 054 and IRMM 49d CRM. The ²⁴²Pu/²³⁵U ratio in the spike was calculated using
234 weighed CRM used for the preparation and the certified ²³⁵U and ²⁴²Pu isotope amount
235 contents. The ²⁴²Pu/²³⁵U spike characteristics are: ²³⁸U/²³⁵U = 0.058065(69),
236 ²³⁸Pu/²⁴²Pu = 0.0053313(35) and ²⁴²Pu/²³⁵U = 0.05074(14).

237 ¹⁵⁰Nd spike solution characterization

238 ¹⁴⁸Nd/²³⁸U ratio determination required using a Nd/U spike. The first step was
239 characterizing the ¹⁵⁰Nd spike solution. For the isotope ratios characterization, 5 deposits
240 of about 10 ng were analyzed with the TE method.

241 The Nd mass fraction was measured by reverse isotope dilution using the NIST 3135a
242 CRM as spike. 3 independent dilutions of the NIST 3135a CRM were performed to obtain
243 Nd mass fraction about 10 μg g⁻¹. Then, 3 (diluted NIST 3135a CRM – ¹⁵⁰Nd spike
244 solution) mixtures were prepared for each dilution cascade. The ¹⁴⁴Nd/¹⁵⁰Nd ratio of each

245 mixture was measured using the TE method to calculate the Nd mass fraction of the ^{150}Nd
246 spike solution. The 3135a CRM being only certified for the mass fraction, these Nd isotope
247 ratios were measured with 5 deposits of about 10 ng using the TE method.

248 *$^{150}\text{Nd}/^{243}\text{Am}/^{235}\text{U}$ spike preparation*

249 $^{241}\text{Am}/^{238}\text{U}$ and $^{148}\text{Nd}/^{238}\text{U}$ ratio were determined in the same experiment with a spike
250 enriched in ^{235}U , ^{243}Am and ^{150}Nd isotopes. This spike, hereafter referred to as
251 $^{150}\text{Nd}/^{243}\text{Am}/^{235}\text{U}$ spike, was prepared gravimetrically from IRMM 054, STAM and ^{150}Nd
252 spike solution. The $^{150}\text{Nd}/^{243}\text{Am}/^{235}\text{U}$ spike characteristic are: $^{238}\text{U}/^{235}\text{U} = 0.058065(69)$,
253 $^{241}\text{Am}/^{243}\text{Am} = 0.135574(54)$, $^{148}\text{Nd}/^{150}\text{Nd} = 0.009906(24)$, $^{243}\text{Am}/^{235}\text{U} = 0.028628(73)$
254 and $^{150}\text{Nd}/^{235}\text{U} = 0.005295(30)$.

255 Analytical protocol

256 An overview of the analytical protocol is summarized in Fig. 1.

257 *Dissolution*

258 The dissolution of MARIOS and DIAMINO discs was conducted in 2 steps in a closed
259 vessel in a hot cell. The primary dissolution was performed in $11 \text{ mol L}^{-1} \text{ HNO}_3$ to dissolve
260 the uranium-based matrix, lanthanides and some of the fission products. The second
261 dissolution step was the residue depletion using ($11 \text{ mol L}^{-1}/0.075 \text{ mol L}^{-1}$) HNO_3/HF
262 mixture added to the primary dissolution solution to quantitatively dissolve the plutonium.
263 Then, two independent 100-fold dilutions were performed for each of the dissolution
264 solution in the hot cell to obtain a radiation level compatible with glove box operations
265 (Fig. 1). Hereafter, the two diluted dissolution solutions are referred to as aliquot 1 and
266 aliquot 2. 3 mL of aliquot 1 and 2 were transferred by pneumatic transfer to the isotopic
267 analyses laboratory.

268 *U isotope ratios measurements*

269 The uranium isotope ratios were measured after a separation on UTEVA resin (Fig. 1).
270 First, 2 mL of (6 mol L⁻¹/0.1 mol L⁻¹) HNO₃/H₂O₂ mixture were added to 300 μL of aliquot
271 1 and 2. This solution (aliquot + HNO₃/H₂O₂ mixture), containing about 15 μg of U, was
272 separated with the UTEVA resin to obtain a purified fraction of U. This fraction was
273 evaporated and dissolved again with 15 μL of 0.5 mol L⁻¹ HNO₃ to obtain a solution with
274 a U mass fraction about 1 μg μL⁻¹. 1 μL (about 1 μg of U) was deposited on 3 filaments
275 for each aliquot to perform the ²³⁵U/²³⁸U ratio determination using the TE method. 4 μL
276 (about 4 μg of U) were deposited on 3 filaments for each aliquot to perform the ²³⁴U/²³⁸U
277 and ²³⁶U/²³⁸U ratios determination using the CMD method. U isotope ratios in each disc
278 are the average from the values acquired for aliquot 1 and 2.

279 *Pu isotope ratios measurements*

280 The Pu isotope ratios were measured after a separation on TEVA resin followed by a
281 separation on UTEVA resin (Fig. 1). First, 2 mL of 8 mol L⁻¹ HNO₃ were added to 300 μL
282 of aliquot 1 and 2. This solution (aliquot + 8 mol L⁻¹ HNO₃), containing about 1 μg of Pu,
283 was separated using the TEVA resin to obtain a Pu fraction purified from Am. The
284 separation on TEVA is also able to purify Pu from U and can be enough to purify Pu from
285 U and Am. However, U traces are commonly observed in the Pu fraction: the
286 decontamination factor is not high enough.

287 The Pu fraction, obtained from the TEVA resin, was evaporated and dissolved again with
288 1 mL of the (6 mol L⁻¹/0.1 mol L⁻¹) HNO₃/H₂O₂ mixture. The UTEVA resin separation
289 protocol was applied to obtain a purified fraction of Pu. This fraction was evaporated and
290 dissolved again with 6 μL of 0.5 mol L⁻¹ HNO₃ to obtain a Pu mass fraction of about
291 200 ng μL⁻¹. 1 μL (about 200 ng of Pu) was deposited on 3 filaments for each aliquot. Pu
292 isotope ratios in each disc are the average from the values acquired for aliquot 1 and 2.

293 *²³⁸Pu/²³⁸U ratio measurements*

294 First each aliquot was diluted 10-fold (Fig. 1). Then, 3 (diluted aliquot - $^{242}\text{Pu}/^{235}\text{U}$ spike)
295 mixtures were prepared and separated using the UTEVA resin to obtain purified fractions
296 of U and Pu. These fractions were evaporated and dissolved again using 10 μL of
297 $0.5 \text{ mol L}^{-1} \text{ HNO}_3$ for the U fraction to obtain U mass fraction about $500 \text{ ng } \mu\text{L}^{-1}$ and using
298 $1 \text{ } \mu\text{L}$ of $0.5 \text{ mol L}^{-1} \text{ HNO}_3$ for the Pu fraction to obtain Pu mass fraction about $400 \text{ ng } \mu\text{L}^{-1}$.
299 $1 \text{ } \mu\text{L}$ (about 500 ng of U and 400 ng of Pu) was deposited on a filament. $^{238}\text{Pu}/^{238}\text{U}$ ratio in
300 each disc is the average value of aliquot 1 and 2.

301 *$^{148}\text{Nd}/^{238}\text{U}$ and $^{241}\text{Am}/^{238}\text{U}$ ratios measurements*

302 2 (aliquot - $^{150}\text{Nd}/^{243}\text{Am}/^{235}\text{U}$ spike) mixtures were prepared for each aliquot. These
303 mixtures, containing about 17 μg of U, 1 μg of Am and 50 ng of Nd, were purified using
304 the TEVA resin to obtain purified fractions of trivalent elements and U (Fig. 1). The
305 trivalent elements fraction was evaporated and then dissolved again in 30 μL of 0.5 mol L^{-1}
306 HNO_3 . This 30 μL was then used to inject 20 μL in the HPLC system. Purified fractions
307 of Am and Nd were obtained and then evaporated. The residue of the Am and Nd fractions
308 was dissolved again with 6 μL and 5 μL of $0.5 \text{ mol L}^{-1} \text{ HNO}_3$, respectively, to obtain a
309 solution with $[\text{Am}] \approx 100 \text{ ng } \mu\text{L}^{-1}$ and $[\text{Nd}] \approx 6 \text{ ng } \mu\text{L}^{-1}$. $1 \text{ } \mu\text{L}$ of solution (about 100 ng of
310 Am and about 6 ng of Nd) was deposited.

311 The U fraction, obtained from the TEVA resin separation, was not well purified against
312 Pu, that interferes the ^{238}U isotope measurement. The U fraction was evaporated and
313 dissolved again with 1 mL of $6 \text{ mol L}^{-1}/0.1 \text{ mol L}^{-1} \text{ HNO}_3/\text{H}_2\text{O}_2$ mixture. The UTEVA
314 resin separation protocol was applied to obtain a purified fraction of U. This fraction was
315 evaporated and dissolved again with 10 μL of $0.5 \text{ mol L}^{-1} \text{ HNO}_3$ to obtain
316 $[\text{U}] \approx 500 \text{ ng } \mu\text{L}^{-1}$ solution. $1 \text{ } \mu\text{L}$ of solution (about 500 ng of U) was deposited.
317 $^{241}\text{Am}/^{238}\text{U}$ and $^{148}\text{Nd}/^{238}\text{U}$ ratios in each disc are the average value of aliquot 1 and 2.

318 **Results evaluation**

319 Bias, or trueness, was calculated using Eq. (2).

$$\text{Bias (\%)} = \frac{Z - \text{ref}}{\text{ref}} \quad (2)$$

320 Where Z is the experimental value and ref is the reference value.

321 Eq. (3) was used to determine if the analytical method has a statistically significant bias. If
322 the normalized error (E_N) is lower than 2, the method is considered having no statistically
323 significant bias [32].

$$E_N = \frac{|Z - \text{ref}|}{\sqrt{u_z^2 + u_{\text{ref}}^2}} \quad (3)$$

324 Where u_z is the measurement uncertainty and u_{ref} is the reference value uncertainty with a
325 coverage factor at $k = 1$.

326 Uncertainties estimation

327 *Isotope ratio uncertainty*

328 The isotope ratio (R) uncertainty (u) at $k = 1$ was estimated using Eq. (4) [14].

$$\frac{u^2(R)}{(R)^2} = \frac{u_{\bar{x}}^2}{(\bar{x})^2} + \frac{u_{\text{trueness}}^2}{(\text{trueness})^2} + \frac{u_{\text{ref}}^2}{(\text{ref})^2} \quad (4)$$

329

$$\frac{u_{\text{trueness}}}{\text{trueness}} = \frac{\text{maximum bias in CRM}}{\sqrt{3}} \quad (5)$$

330 The first term of Eq. (4) on right hand side is given by the Relative Standard Deviation
331 (RSD, *i.e.* random effects). The second and third terms take into account the systematic
332 effect. The measurement trueness is calculated using Eq. (5) with a reference material. The
333 optimal reference material is the same element as the analyte with similar isotope ratio.
334 The 2019UPuNH sample was used to evaluate the $^{235}\text{U}/^{238}\text{U}$ isotope ratio: ratio about

335 0.0074 for the material and about 0.004 for both discs. The IRMM 187 was used for the
336 $^{234}\text{U}/^{238}\text{U}$ and $^{236}\text{U}/^{238}\text{U}$ isotope ratios.

337 The Pu isotope ratios were evaluated with the 2017PuNH and 2019UPuNH materials. The
338 choice of the material is not very important in this case as similar biases were observed
339 during ILC: the only difference is 2019UPuNH has lowest assigned values uncertainties
340 than 2017PuNH. The choice of the material was only made to be as close as possible to the
341 measurement values of the discs. The $^{242}\text{Pu}/^{239}\text{Pu}$ ratio of the 2019UPuNH (about 0.03)
342 was used for the $^{242}\text{Pu}/^{238}\text{Pu}$ uncertainty estimation in the discs (about 0.2). The $^{240}\text{Pu}/^{239}\text{Pu}$
343 ratio of 2017PuNH sample (about 0.1) was used for the $^{239}\text{Pu}/^{238}\text{Pu}$ (0.1-0.2) and
344 $^{240}\text{Pu}/^{238}\text{Pu}$ (0.01-0.03) uncertainty estimations in the discs. The $^{241}\text{Pu}/^{239}\text{Pu}$ ratio of
345 2017PuNH sample (about 0.002) was used for the $^{241}\text{Pu}/^{238}\text{Pu}$ ratio in the discs (0.002-
346 0.01).

347 *Double isotope dilution uncertainty*

348 $^{238}\text{Pu}/^{238}\text{U}$, $^{241}\text{Am}/^{238}\text{U}$ and $^{148}\text{Nd}/^{238}\text{U}$ ratios uncertainties were estimated by combining
349 the uncertainties from each term of the DID equation. A precision component was added
350 and corresponds to the RSD obtained for the two aliquots divided by the square root of the
351 number of aliquots (here 2).

352 **Results and discussion**

353 **Analytical optimization**

354 *Pu purification against Am*

355 Routinely the Pu purification is performed in one separation step with the UTEVA resin
356 first. This protocol was applied for one of the DIAMINO aliquot. The repeatability
357 observed for the 3 measurements of the $^{241}\text{Pu}/^{238}\text{Pu}$ ratio coming from the same separation
358 was 16 %, which is important for isotope ratio about 0.002. Fig. 2.a shows the $^{241}\text{Pu}/^{238}\text{Pu}$

359 ratio evolution as a function of time (or cycle number) while using the TE method. The
360 ratio mainly decrease during the TE method, which is not in agreement with the isotope
361 fractionation law. Lighter isotopes mainly evaporate at the beginning of the TE method
362 compared to the heavier isotopes: the $^{241}\text{Pu}/^{238}\text{Pu}$ ratio need to increase during the TE
363 method to respect the isotope fractionation law. These informations (repeatability and
364 profile) showed ^{241}Pu isotope measurement is interfered by the ^{241}Am isotope after one
365 separation step with UTEVA resin.

366 To solve this Pu/Am interference, a separation using a TEVA resin was added before the
367 UTEVA resin separation. The $^{241}\text{Pu}/^{238}\text{Pu}$ ratio thus obtained is 27 % lower than the value
368 obtained after only a UTEVA resin separation. The repeatability observed for the 3
369 measurements coming from the same separation improves to 0.2 % for DIAMINO and
370 MARIOS measurements (Table 2). Fig. 2.b shows the $^{241}\text{Pu}/^{238}\text{Pu}$ ratio evolution as a
371 function of time while using the TE method for a DIAMINO aliquot after TEVA and
372 UTEVA separation. The ratio increases slowly, which is in agreement with the isotope
373 fractionation law. The repeatability and the $^{241}\text{Pu}/^{238}\text{Pu}$ ratio evolution during the TE
374 method showed combining TEVA and UTEVA resins is efficient to overcome the
375 $^{241}\text{Am}/^{241}\text{Pu}$ isobaric interference.

376 This behavior difference between the routine samples and the MARIOS/DIAMINO discs
377 can be explained by the Am/Pu ratio. The routine samples contained more Pu than Am: the
378 Am/Pu ratio is mainly below 0.1. For the DIAMINO and MARIOS discs, the Am/Pu ratio
379 was about 1. The trivalent elements decontamination used routinely using the UTEVA
380 resin separation is probably not sufficient to eliminate this higher Am quantity.

381 *U purification against Pu*

382 The absence of Pu in the U fraction was verified by measuring the ^{239}Pu isotope for each
383 U analysis. The $^{239}\text{Pu}/^{238}\text{U}$ ratio is an indicator of the U/Pu purification efficacy. The
384 highest $^{239}\text{Pu}/^{238}\text{U}$ ratio observed during the measurements was 3×10^{-5} (Table 2) which is
385 slightly higher than the detection limit estimated to 1×10^{-5} [17]. Combining the $^{239}\text{Pu}/^{238}\text{Pu}$
386 ratio measured during the Pu isotope ratios determination (about 0.1 for DIAMINO disc

387 and 0.2 for MARIOS disc) and the $^{239}\text{Pu}/^{238}\text{U}$ ratio measured here, the contribution of the
388 ^{238}Pu isotope to the signal measured at mass 238 amu has been calculated at about 0.02 %
389 and is negligible compared to the repeatability (RSD about 0.1 % for both discs, Table 2)
390 and the estimated uncertainty (relative uncertainty is over 0.16 % for all U isotope ratios).
391 $^{235}\text{U}/^{238}\text{U}$ isotope ratio evolution during the TE method was also verified for each analysis
392 and confirmed the separation efficiency.

393 *Pu purification against U*

394 The absence of U in the Pu fraction can be verified by measuring the ^{235}U isotope for each
395 Pu analysis. The highest $^{235}\text{U}/^{238}\text{Pu}$ ratio observed was lower than the detection limit and
396 estimated to 5.10^{-5} (Table 2). This value gives a first approximation of the Pu purification
397 quality. However, ^{235}U isotope is not abundant enough ($^{235}\text{U}/^{238}\text{U}$ ratio of about 0.004 for
398 both discs) to make sure the Pu fraction contained no traces of U. $^{235}\text{U}/^{238}\text{Pu}$ ratio is not the
399 perfect indicator as was, previously, the $^{239}\text{Pu}/^{238}\text{U}$ ratio for the U purification control. Pu
400 isotope ratios evolution while using the TE method was verified for each Pu analysis and
401 for each Pu isotope ratio to make sure the ratio evolution are in agreement with the isotope
402 fractionation law. These observations confirmed the separation quality to obtain a Pu
403 purified from U.

404 *Method validation for $^{234}\text{U}/^{238}\text{U}$ and $^{236}\text{U}/^{238}\text{U}$ isotope ratios* 405 *determination using the CMD method with the FC 13*

406 The updated parameters for the CMD method were validated using the IRMM 187 CRM.
407 The biases obtained are equal to -0.003 % for the $^{234}\text{U}/^{238}\text{U}$ ratio and to -0.004 % for the
408 $^{236}\text{U}/^{238}\text{U}$ ratio. The RSD for the $^{234}\text{U}/^{238}\text{U}$ and $^{236}\text{U}/^{238}\text{U}$ ratios are equal to 0.04 % and
409 0.06 %, respectively. The normalized error calculated for both isotope ratios ($E_N = 0.07$ for
410 $^{234}\text{U}/^{238}\text{U}$ ratio and $E_N = 0.05$ for $^{236}\text{U}/^{238}\text{U}$ ratio) were below 2, showing the method has
411 no significant bias and validating the updated parameters for minor U isotope ratios
412 determination.

413 ¹⁵⁰Nd spike calibration

414 The ¹⁵⁰Nd spike calibration is composed of 3 steps: isotope ratios determination of the
415 NIST 3135a CRM used as spike, isotope ratios determination of the ¹⁵⁰Nd spike and mass
416 fraction determination of the ¹⁵⁰Nd spike by reserve isotope dilution.

417 The Nd isotope ratios of the NIST 3135a CRM correspond to a natural Nd (see Table S1
418 in the supplementary information). The repeatability observed for all isotope ratios were
419 below 0.05 %. The uncertainties were estimated between 0.1 and 0.3 % (k = 2).

420 The Nd isotope ratios of the ¹⁵⁰Nd spike were summarized in Table S2 in the supplementary
421 information. The repeatability observed for all isotope ratios (RSD between 0.1% to 0.7 %)
422 were higher than the ones observed for natural uranium (RSD < 0.1 %), due to lower
423 isotope ratios in the case of the ¹⁵⁰Nd spike. The uncertainty were estimated between 0.3 %
424 and 1.3 % (k = 2).

425 The Nd mass fraction of the ¹⁵⁰Nd spike was determined at 7.468(40) µg g⁻¹. The
426 repeatability among the 3 independent determinations was 0.13 %. The uncertainty was
427 estimated to 0.53 % (k = 2). The study of the main uncertainty sources shows the total
428 uncertainty is mainly due to the Nd mass fraction uncertainty of the NIST 3135a CRM
429 (69 % of the total uncertainty). The others uncertainty sources are the mixture isotope ratio
430 uncertainty (11 % of the total uncertainty), the masses uncertainties (10 % of the total
431 uncertainty) and the repeatability (10 % of the total uncertainty). The other uncertainty
432 sources, like Nd isotope ratios of the 3135a CRM and ¹⁵⁰Nd spike, are negligible (below
433 1 % of the total uncertainty). These measurements calibrated the ¹⁵⁰Nd spike for isotope
434 ratios and mass fraction.

435 Results of MARIOS and DIAMINO discs

436 Results are summarized in Table 3.

437 *U isotope ratios*

438 The $^{235}\text{U}/^{238}\text{U}$ ratio was 0.0045960(85) for the DIAMINO disc and 0.0041534(69) for the
439 MARIOS discs. The repeatability between the two aliquots were equal to 0.06 % for the
440 DIAMINO disc and 0.01 % for the MARIOS disc. The relative uncertainties were 0.18 %
441 and 0.17 % for DIAMINO and MARIOS discs, respectively.

442 The $^{234}\text{U}/^{238}\text{U}$ ratio was 0.0019338(37) for the DIAMINO disc and 0.005052(12) for the
443 MARIOS discs. The $^{236}\text{U}/^{238}\text{U}$ ratio was 0.0004201(11) for the DIAMINO disc and
444 0.0005800(19) for the MARIOS disc. The repeatabilities were below 0.2 %. The relative
445 uncertainties were estimated between 0.19 % and 0.33 %.

446 *Pu isotope ratios*

447 $^{239}\text{Pu}/^{238}\text{Pu}$, $^{240}\text{Pu}/^{238}\text{Pu}$ and $^{242}\text{Pu}/^{238}\text{Pu}$ ratios were 0.12101(17), 0.015288(54) and
448 0.21275(45), respectively, for the DIAMINO disc and 0.20247(17), 0.030771(29) and
449 0.20240(36), respectively, for the MARIOS disc. The relative uncertainties were between
450 0.09 % and 0.35 %.

451 $^{241}\text{Pu}/^{238}\text{Pu}$ ratio were measured at 0.002129(13) and 0.011497(66) for DIAMINO and
452 MARIOS discs, respectively. The relative uncertainty (about 0.6 % for both disc) were
453 higher than the other Pu isotope ratios (below 0.35 %). This is explained by the material
454 chosen to calculate the systematic effect in the uncertainty equation: this material (*i.e.*
455 2017PuNH sample) have an uncertainty of 0.53 % ($k = 2$) whereas the material used to
456 calculate the systematic effect for others isotope ratios have an uncertainty below 0.04 %
457 ($k = 2$).

458 *$^{238}\text{Pu}/^{238}\text{U}$, $^{241}\text{Am}/^{238}\text{U}$ and $^{148}\text{Nd}/^{238}\text{U}$ isotope ratios*

459 The $^{238}\text{Pu}/^{238}\text{U}$ ratio is 0.04887(18) for the DIAMINO disc and 0.07980(30) for the
460 MARIOS disc. The repeatabilities are below 0.1 % for both disc. The relative uncertainties
461 were estimated at 0.35 % for the DIAMINO disc and 0.37 % for the MARIOS disc ($k = 2$).
462 The study of the main uncertainty sources shows that the total uncertainty is mainly come
463 from the $^{242}\text{Pu}/^{235}\text{U}$ ratio of the spike (about 58 % of the total uncertainty), the $^{238}\text{U}/^{235}\text{U}$

464 mixture ratio (about 18 % of the total uncertainty) and $^{238}\text{Pu}/^{242}\text{Pu}$ mixture ratio (about
465 22 % of the total uncertainty). The others uncertainty sources (sample and spike isotope
466 ratios) are negligible (below 2 % of the total uncertainty).

467 The $^{241}\text{Am}/^{238}\text{U}$ ratios were measured at 0.08545(29) and 0.06242(23) for DIAMNIO and
468 MARIOS discs, respectively. The repeatabilities are below 0.1 % for both discs. The
469 relative uncertainties are estimated at 0.34 % and 0.37 % for DIAMNIO and MARIOS
470 discs, respectively. As for the $^{238}\text{Pu}/^{238}\text{U}$, the study of the main uncertainty sources shows
471 that the total uncertainty is mostly come from the $^{243}\text{Am}/^{235}\text{U}$ ratio of the spike (about 57 %
472 of the total uncertainty), the $^{238}\text{U}/^{235}\text{U}$ mixture ratio (about 19 % of the total uncertainty)
473 and the $^{241}\text{Am}/^{243}\text{Am}$ mixture ratio (about 23 % of the total uncertainty). The others
474 uncertainty sources are negligible (below 1 % of the total uncertainty).

475 The $^{148}\text{Nd}/^{238}\text{U}$ ratio was determined at 0.0002153(14) for the DIAMINO disc and
476 0.0004805(33) for the MARIOS disc. The repeatabilities are about 0.2 % for both disc. The
477 relative uncertainties were estimated at 0.65 % and 0.68 % for DIAMNIO and MARIOS
478 discs, respectively. These uncertainties are about twice higher than the ones estimated for
479 $^{238}\text{Pu}/^{238}\text{U}$ and $^{241}\text{Am}/^{238}\text{U}$ ratios (about 0.35 %). This is mainly due to the $^{150}\text{Nd}/^{235}\text{U}$ ratio
480 uncertainty of the spike that is estimated to 0.57 % ($k = 2$). It is mathematically impossible
481 to obtain a $^{148}\text{Nd}/^{238}\text{U}$ ratio uncertainty below the $^{150}\text{Nd}/^{235}\text{U}$ spike ratio uncertainty. The
482 study of the main uncertainty sources shows that the contribution linked to the $^{150}\text{Nd}/^{235}\text{U}$
483 spike ratio increased: about 75 % of the total uncertainty for the $^{148}\text{Nd}/^{238}\text{U}$ ratio compared
484 to about 60 % for $^{238}\text{Pu}/^{238}\text{U}$ and $^{241}\text{Am}/^{238}\text{U}$ ratios.

485 Comparison between analysis results and neutron simulation ones

486 The information provided in Table 3 indicate a rather good agreement between analysis
487 results and neutron simulation ones.

488 In the case of DIAMINO, almost all the deviations remain below 20 % which is satisfactory
489 considering all uncertainties associated to both neutron simulations and analysis
490 measurements. Only the deviation related to the ratio $^{241}\text{Pu}/^{238}\text{Pu}$ is higher (34 %), possibly

491 due to uncertainties in some specific neutron cross-sections used in neutron simulations
492 where the neutron flux has the OSIRIS reactor particular energy spectrum.

493 As for MARIOS, more deviations exceed 20 %. The ones related to specific isotopes in the
494 isotopic vector of an element (*i.e.* $^{234}\text{U}/^{238}\text{U}$, $^{240}\text{Pu}/^{238}\text{Pu}$ and $^{241}\text{Pu}/^{238}\text{Pu}$) could also be due
495 to neutron cross-section uncertainties. Regarding the $^{148}\text{Nd}/^{238}\text{U}$ and $^{241}\text{Am}/^{238}\text{U}$ ratios, the
496 slight lack of neodymium and excess of americium as-calculated suggest that neutron
497 calculations were run up till a slightly lower fluence compared to the experimental one. In
498 addition, it is mentioned that the fluence used in the MARIOS neutron calculations
499 corresponds to the one determined from measurements performed on the activation monitor
500 set of the irradiation device, some uncertainties being also associated to these
501 measurements.

502 **Conclusions**

503 Six discs from MARIOS and DIAMINO irradiations experiments were dissolved in a hot
504 cell before analysis. These analyses are part of an R&D program initiated in 2008 at the
505 CEA on minor actinides transmutation. Isotopic analyses were carried out with high
506 accuracy to help interpreting the experiments and to qualify the associated evolution
507 calculation code for different isotopes. Several analytical optimizations of the protocol
508 were performed.

509 The Pu purification was optimized to ensure an optimal Pu/Am separation. Adding a TEVA
510 resin separation before the usually employed UTEVA resin separation helps measuring the
511 ^{241}Pu isotope without any interference from the ^{241}Am isotope. The DID showed its
512 potential for the $^{238}\text{Pu}/^{238}\text{U}$, $^{241}\text{Am}/^{238}\text{U}$ and $^{148}\text{Nd}/^{238}\text{U}$ ratios determination. Compared to
513 the conventional ID-TIMS methodology, the DID showed lower uncertainties: estimated
514 to a few percent for the ID-TIMS and to a few per mil for the double isotope dilution. The
515 DID is also faster as no gravimetrically preparation are required as this step is tedious in
516 hot cell or in glove box.

517 Uncertainties, estimated about a few per mil for the main determination, showed significant
518 difference between discs of the same irradiation. The burnup of each disc is slightly
519 different depending on the position of the disc in the needle (bottom, middle or high), that
520 produce different transmutation yield and isotope ratios.

521 **Acknowledgements**

522 We are grateful to Dr. S. Baghdadi (CEA/DES/ISEC/DMRC/SASP/L2AT) for her
523 precious advice on the present paper. We would like to thank Dr. Eric Esbelin, Dr. Steve
524 Jan, Ms Barbara Caniffi, Ms Corinne Deshoux, Ms Delphine Vantalou, Mr Bruce Charles,
525 Mr Regis Joulia, Mr Laurent Lancial, Mr Lyonel Trintignac
526 (CEA/DES/ISEC/DMRC/SASP/L2AT) and Mr Ygor Davrain
527 (CEA/DES/ISEC/CETAMA) who have taken part in this work.

528 **Table**

529 Table 1: Summarized description of one cycle of the CMD method

Cups Detectors	L2 FC 13	L1 FC 12	C SEM	H1 FC 11	H2 FC 11	Integration number	Measurement time (s)	Idle time (s)
Sequence 1	²³⁴ U	²³⁵ U	²³⁶ U		²³⁸ U	3	8	1
Sequence 2			²³⁴ U	²³⁵ U		3	8	1
Sequence 3	233.7	234.7	235.7		237.7	3	4	5
Sequence 4	234.4	235.4	236.4		238.4	3	4	1

530

531

532

533 Table 2: ²³⁹Pu/²³⁸U maximal ratio and RSD obtained for the ²³⁵U/²³⁸U ratio during U
 534 analysis and ²³⁵U/²³⁸Pu maximal ratio and RSD obtained for the ²⁴¹Pu/²³⁸Pu ratio during
 535 Pu analysis for aliquot 1 and 2 of DIAMINO and MARIOS discs

Disc	Aliquot	U analysis		Pu analysis	
		²³⁹ Pu/ ²³⁸ U	RSD ²³⁵ U/ ²³⁸ U	²³⁵ U/ ²³⁸ Pu	RSD ²⁴¹ Pu/ ²³⁸ Pu
DIAMINO	1	2.1×10 ⁻⁵	0.14 %	< 1×10 ⁻⁵	0.12 %
	2	3.0×10 ⁻⁵	0.10 %	< 1×10 ⁻⁵	0.14 %
MARIOS	1	2.3×10 ⁻⁵	0.04 %	< 1×10 ⁻⁵	0.01 %
	2	2.0×10 ⁻⁵	0.05 %	< 1×10 ⁻⁵	0.04 %

536

537

538

539 Table 3: Experimental and neutronic simulation results for the DIAMINO and MARIOS
 540 discs. Values in parenthesis are the estimated uncertainties expressed at $k = 2$

Isotope ratio	DIAMINO disc	DIAMINO neutronic simulation	MARIOS disc	MARIOS neutronic simulation
$^{234}\text{U}/^{238}\text{U}$	0.0019338(37)	0.00232	0.005052(12)	0.00281
$^{235}\text{U}/^{238}\text{U}$	0.0045960(85)	0.00490	0.0041534(69)	0.00433
$^{236}\text{U}/^{238}\text{U}$	0.0004201(11)	0.00045	0.0005800(19)	0.00053
$^{239}\text{Pu}/^{238}\text{Pu}$	0.12101(17)	0.114	0.20247(17)	0.185
$^{240}\text{Pu}/^{238}\text{Pu}$	0.015288(54)	0.0187	0.030771(29)	0.0223
$^{241}\text{Pu}/^{238}\text{Pu}$	0.002129(13)	0.0030	0.011497(66)	0.0094
$^{242}\text{Pu}/^{238}\text{Pu}$	0.21275(45)	0.214	0.20240(36)	0.208
$^{238}\text{Pu}/^{238}\text{U}$	0.04887(18)	0.0497	0.07980(30)	0.0690
$^{241}\text{Am}/^{238}\text{U}$	0.08545(29)	0.0873	0.06242(23)	0.0845
$^{148}\text{Nd}/^{238}\text{U}$	0.0002153(14)	0.00022	0.0004805(33)	0.00035

541

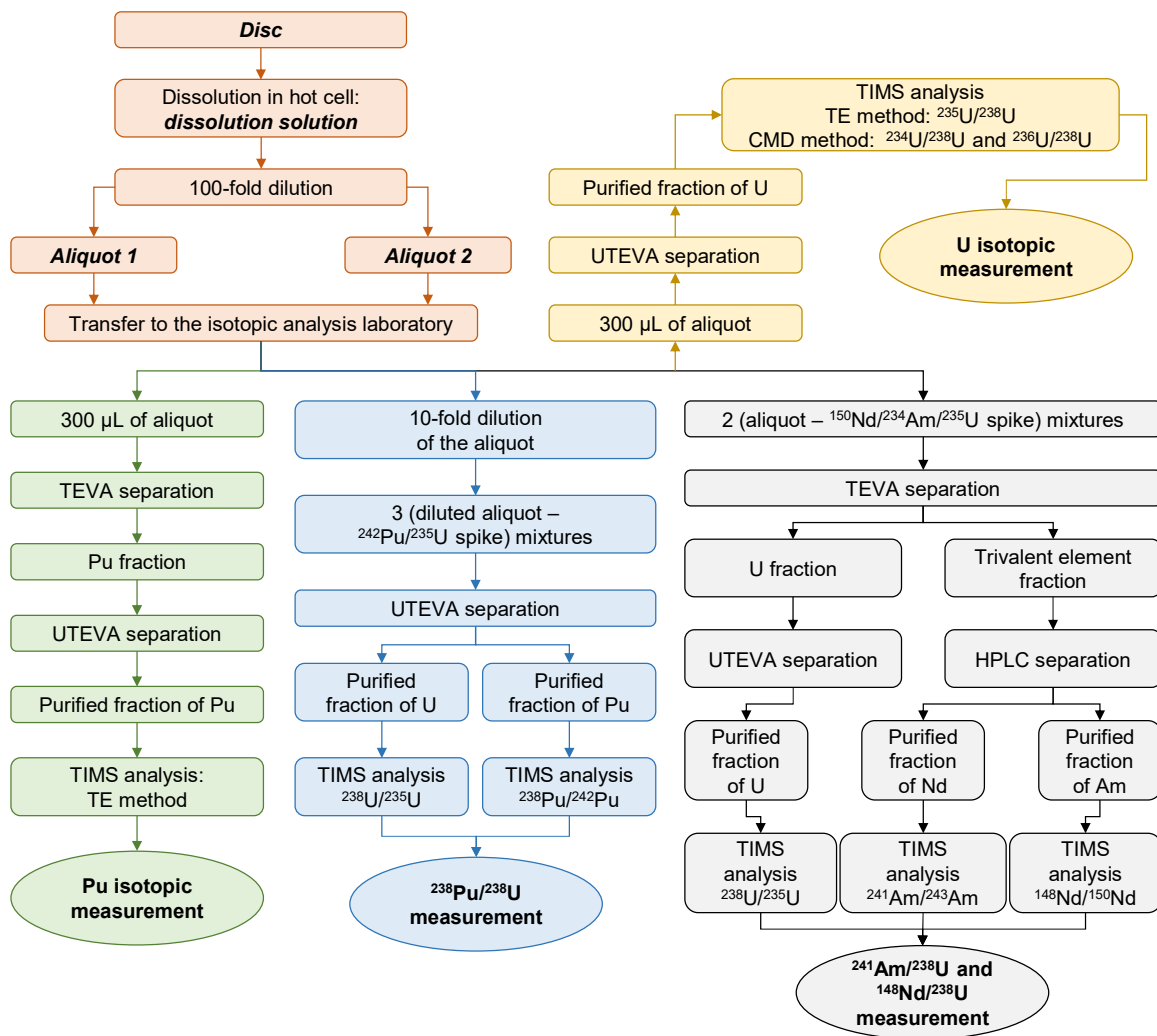
542

543

544

545

Figure



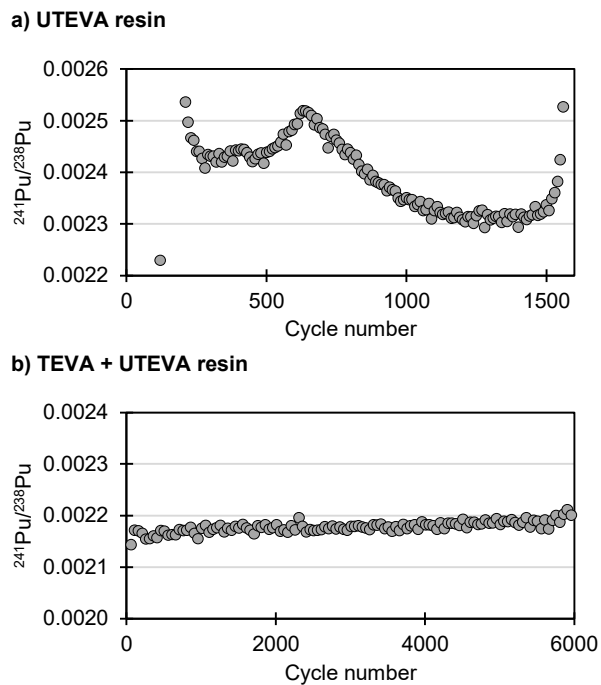
546

547

Fig. 1: Schematics of the analytical protocol

548

549



550

551 Fig. 2: $^{241}\text{Pu}/^{238}\text{Pu}$ isotope ratio evolution through an analysis by the TE method for the
552 DIAMINO aliquot 1 after a UTEVA resin separation (a) and after a TEVA resin
553 separation following by UTEVA resin separation (b). For better clarity only 1 in 10
554 points (a) and 1 in 50 points (b) were plotted

555

556 **References**

- 557 1. Bejaoui S, Helfer T, Bendotti S, Lambert T (2019) Description and thermal
558 simulation of the DIAMINO irradiation experiment of transmutation fuel in the
559 OSIRIS reactor. Prog Nucl Energy 113:28–44.
560 <https://doi.org/10.1016/j.pnucene.2019.01.012>
- 561 2. Bejaoui S, Bendotti S, Lambert T, Helfer T (2017) Status of the DIAMINO
562 experiment irradiated in the OSIRIS reactor. In: Proceedings of GLOBAL 2017.
563 Seoul (Korea)
- 564 3. D’Agata E, Hania PR, Bejaoui S, Sciolla C, Wyatt T, Hannink MHC, Herlet N,
565 Jankowiak A, Klaassen FC, Lapetite JM, Boomstra DA, Phelip M, Delage F (2013)
566 The results of the irradiation experiment MARIOS on americium transmutation.
567 Ann Nucl Energy 62:40–49. <https://doi.org/10.1016/j.anucene.2013.05.043>
- 568 4. Horlait D, Lebreton F, Delahaye T, Herlet N, Dehaut P (2012) $U_{1-x}Am_xO_{2\pm\delta}$
569 MABB Fabrication in the Frame of the DIAMINO Irradiation Experiment. Procedia
570 Chem 7:485–492. <https://doi.org/10.1016/j.proche.2012.10.074>
- 571 5. Prieur D, Jankowiak A, Delahaye T, Herlet N, Dehaut P, Blanchart P (2011)
572 Fabrication and characterisation of $U_{0.85}Am_{0.15}O_{2-x}$ discs for MARIOS
573 irradiation program. J Nucl Mater 414:503–507.
574 <https://doi.org/10.1016/j.jnucmat.2011.05.036>
- 575 6. Beauvy M, Berthoud G, Defranceschi M, Ducros G, Guérin Y, Latgé C, Limoge Y,
576 Madic C, Moisy P, Santarani G, Seiler J-M, Sollogoub P, Vernaz E (2008)
577 Treatment and recycling of spent nuclear fuel, Actinide partitioning - application to
578 waste management, Le Moniteur Editions, Paris, France
- 579 7. (2018) State-of-the-art Report on the Progress of Nuclear Fuel Cycle Chemistry.
580 OECD
- 581 8. Quemet A, Sevilla J, Vauchy R (2021) A combined TIMS and ICP-MS study for

- 582 Th_{0.5}Np_{0.5}O₂ thorium neptunium mixed oxide analysis. *Int J Mass Spectrom*
583 460:116479. <https://doi.org/10.1016/j.ijms.2020.116479>
- 584 9. Quemet A, Maloubier M, Ruas A (2016) Contribution of the Faraday cup coupled
585 to 1012 ohms current amplifier to uranium 235/238 and 234/238 isotope ratio
586 measurements by Thermal Ionization Mass Spectrometry. *Int J Mass Spectrom*
587 404:35–39. <https://doi.org/10.1016/j.ijms.2016.04.005>
- 588 10. Quemet A, Maloubier M, Dalier V, Ruas A (2014) Development of an analysis
589 method of minor uranium isotope ratio measurements using electron multipliers in
590 thermal ionization mass spectrometry. *Int J Mass Spectrom* 374:26–32.
591 <https://doi.org/10.1016/j.ijms.2014.10.008>
- 592 11. Bürger S, Riciputi LR, Bostick DA, Turgeon S, McBay EH, Lavelle M (2009)
593 Isotope ratio analysis of actinides, fission products, and geolocators by high-
594 efficiency multi-collector thermal ionization mass spectrometry. *Int J Mass*
595 *Spectrom* 286:70–82
- 596 12. Bürger S, Balsley SD, Baumann S, Berger J, Boulyga SF, Cunningham JA, Kappel
597 S, Koepf A, Poths J (2012) Uranium and plutonium analysis of nuclear material
598 samples by multi-collector thermal ionisation mass spectrometry: Quality control,
599 measurement uncertainty, and metrological traceability. *Int J Mass Spectrom*
600 311:40–50
- 601 13. Aggarwal SK (2016) Thermal ionisation mass spectrometry (TIMS) in nuclear
602 science and technology – a review. *Anal Methods* 8:942–957.
603 <https://doi.org/10.1039/c5ay02816g>
- 604 14. Quemet A, Ruas A, Dalier V, Rivier C (2018) Americium isotope analysis by
605 Thermal Ionization Mass Spectrometry using the Total Evaporation Method. *Int J*
606 *Mass Spectrom* 431:8–14. <https://doi.org/10.1016/j.ijms.2018.05.017>
- 607 15. Aggarwal SK (2018) A review on the mass spectrometric studies of americium:
608 Present status and future perspective. *Mass Spectrom Rev* 37:43–56.

- 609 <https://doi.org/10.1002/mas.21506>
- 610 16. Guéguen F, Isnard H, Nonell A, Vio L, Vercoüter T, Chartier F (2015) Neodymium
611 isotope ratio measurements by LC-MC-ICPMS for nuclear applications:
612 investigation of isotopic fractionation and mass bias correction. *J Anal At Spectrom*
613 30:443–452. <https://doi.org/10.1039/C4JA00361F>
- 614 17. Quemet A, Ruas A, Dalier V, Rivier C (2019) Development and comparison of high
615 accuracy thermal ionization methods for uranium isotope ratios determination in
616 nuclear fuel. *Int J Mass Spectrom* 438:166–174.
617 <https://doi.org/10.1016/j.ijms.2019.01.008>
- 618 18. Quemet A, Buravand E, Catanese B, Huot P, Dalier V, Ruas A (2020) Monitoring
619 the dissolution of a uranium-plutonium oxide from a spent fuel solution: using
620 plutonium ratio and TIMS for isotope ratio measurements. *J Radioanal Nucl Chem*
621 326:255–260. <https://doi.org/10.1007/s10967-020-07311-5>
- 622 19. Quemet A, Angenieux M, Ruas A (2021) Nd, Am and Cm isotopic measurement
623 after simultaneous separation in transmutation irradiated samples. *J Anal At*
624 *Spectrom* 36:1758. <https://doi.org/10.1039/D1JA00165E>
- 625 20. Horwitz EP, Dietz ML, Chiarizia R, Diamond H, Maxwell SL, Nelson MR (1995)
626 Separation and Preconcentration of Actinides by Extraction Chromatography Using
627 a Supported Liquid Anion-Exchanger - Application to the Characterization of High-
628 Level Nuclear Waste Solutions. *Anal Chim Acta* 310:63–78.
629 [https://doi.org/10.1016/0003-2670\(95\)00144-O](https://doi.org/10.1016/0003-2670(95)00144-O)
- 630 21. Morgenstern A, Apostolidis C, Carlos-Marquez R, Mayer K, Molinet R (2002)
631 Single-column extraction chromatographic separation of U, Pu, Np and Am.
632 *Radiochim Acta* 90:81–85. https://doi.org/10.1524/ract.2002.90.2_2002.81
- 633 22. Apostolidis C, Molinet R, Richir P, Ougier M, Mayer K (1998) Development and
634 Validation of a Simple, Rapid and Robust Method for the Chemical Separation of
635 Uranium and Plutonium. *Radiochim Acta* 83:21–25.

- 636 <https://doi.org/10.1524/ract.1998.83.1.21>
- 637 23. Goutelard F, Caussignac C, Brennetot R, Stadelmann G, Gautier C (2009)
638 Optimization conditions for the separation of rare earth elements, americium,
639 curium and cesium with HPLC technique. *J Radioanal Nucl Chem* 282:669–675.
640 <https://doi.org/10.1007/s10967-009-0308-z>
- 641 24. Banik N Lal, Lützenkirchen K, Malmbeck R, Nichol A (2019) A method for the mg
642 scale separation of curium(III) from americium(III) by HPLC using a SCX column.
643 *J Radioanal Nucl Chem* 321:841–849. <https://doi.org/10.1007/s10967-019-06653-z>
- 644 25. Quemet A, Maillard C, Ruas A (2015) Determination of zirconium isotope
645 composition and concentration for nuclear sample analysis using Thermal Ionization
646 Mass Spectrometry. *Int J Mass Spectrom* 392:34–40.
647 <https://doi.org/10.1016/j.ijms.2015.08.023>
- 648 26. Quemet A, Ruas A, Esbelin E, Dalier V, Rivier C (2019) Development and
649 comparison of two high accuracy methods for uranium concentration in nuclear fuel:
650 ID-TIMS and K-edge densitometry. *J Radioanal Nucl Chem* 321:997–1004.
651 <https://doi.org/10.1007/s10967-019-06670-y>
- 652 27. International Atomic Energy Agency (2010) International Target Values 2010 for
653 Measurement Uncertainties in Safeguarding Nuclear Materials - STR368. Vienna,
654 Austria
- 655 28. Désenfant M, Priel M (2017) Reference and additional methods for measurement
656 uncertainty evaluation. *Measurement* 95:339–344.
657 <https://doi.org/10.1016/j.measurement.2016.10.022>
- 658 29. Chartier F, Aubert M, Pilier M (1999) Determination of Am and Cm in spent nuclear
659 fuels by isotope dilution inductively coupled plasma mass spectrometry and isotope
660 dilution thermal ionization mass spectrometry after separation by high-performance
661 liquid chromatography. *Fresenius J Anal Chem* 364:320–327
- 662 30. Henri Becquerel National Laboratory (2015) Mini Table of radionuclides, First

663 edition. EDP Sciences

664 31. Quemet A, Baghdadi S (2021) Optimization of the double isotope dilution. J Anal
665 At Spectrom under peer review

666 32. Désenfant M, Priel M, Rivier C (2005) Evaluation des incertitudes des résultats
667 d'analyse. Ref P105 V1. Les Tech l'Ingénieur 1–17

668